APL Materials

Comparison of thermoelectric properties of nanostructured Mg_2Si, $FeSi_2$, SiGe, and nanocomposites of SiGe–Mg_2Si, SiGe–$FeSi_2$

Cite as: APL Mater. **4**, 104814 (2016); https://doi.org/10.1063/1.4966138
Submitted: 10 May 2016 • Accepted: 06 October 2016 • Published Online: 28 October 2016

Amin Nozariasbmarz, Palash Roy, Zahra Zamanipour, et al.

Comparison of thermoelectric properties of nanostructured Mg_2Si, $FeSi_2$, SiGe, and nanocomposites of SiGe–Mg_2Si, SiGe–$FeSi_2$

Amin Nozariasbmarz,[1,2] Palash Roy,[3] Zahra Zamanipour,[3]
J. Houston Dycus,[2] Matthew J. Cabral,[2] James M. LeBeau,[2]
Jerzy S. Krasinski,[3] and Daryoosh Vashaee[1,2,a]
[1]*Department of Electrical and Computer Engineering, Monteith Research Center, North Carolina State University, Raleigh, North Carolina 27606, USA*
[2]*Department of Materials Science and Engineering, North Carolina State University, Raleigh, North Carolina 27695, USA*
[3]*School of Electrical and Computer Engineering, Helmerich Advanced Technology Research Center, Oklahoma State University, Tulsa, Oklahoma 74106, USA*

(Received 10 May 2016; accepted 6 October 2016; published online 28 October 2016)

Thermoelectric properties of nanostructured $FeSi_2$, Mg_2Si, and SiGe are compared with their nanocomposites of SiGe–Mg_2Si and SiGe–$FeSi_2$. It was found that the addition of silicide nanoinclusions to SiGe alloy maintained or increased the power factor while further reduced the thermal conductivity compared to the nanostructured single-phase SiGe alloy. This resulted in ZT enhancement of $Si_{0.88}Ge_{0.12}$–$FeSi_2$ by ~30% over the broad temperature range of 500-950 °C compared to the conventional $Si_{0.80}Ge_{0.20}$ alloy. The $Si_{0.88}Ge_{0.12}$–Mg_2Si nanocomposite showed constantly increasing ZT versus temperature up to 950 °C (highest measured temperature) reaching ZT ~ 1.3. These results confirm the concept of silicide nanoparticle-in-SiGe-alloy proposed earlier by Mingo *et al.* [Nano Lett. **9**, 711–715 (2009)].
[http://dx.doi.org/10.1063/1.4966138]

Low dimensional nanostructured thermoelectric materials can potentially increase the thermoelectric figure of merit (ZT) by either reducing the thermal conductivity due to phonons scattering at interfaces or the increase of the thermoelectric power factor.[2] The dimensionless thermoelectric figure of merit is defined as $ZT = S^2\sigma T/\kappa$, where σ, S, κ, and T are the electrical conductivity, Seebeck coefficient, thermal conductivity, and temperature in Kelvin, respectively. The thermoelectric power factor is the $S^2\sigma$ term which depends on the electrical properties of the material.[3,4] The following experiments demonstrated the role of nanostructuring on increasing the figure of merit both in thin films[5] and nanostructured bulk materials.[6] Although nanostructuring of some bulk materials such as BiSbTe,[7] Si,[8] SiGe,[9] and PbSrTe[10] showed significant improvement in ZT, similar trend was not observed in some other materials like Mg_2Si,[11,12] $FeSi_2$[13] and $MnSi_{1.7}$.[14,15]

Multiphase composite materials have been also considered for thermoelectric applications. Thermoelectric properties of a composite material was conceptually studied by Straley in 1981[16] and later by Bergman and Levy in 1991,[17] where they claimed that the ZT of a two-component composite material can never exceed the ZT of each individual component. However, later in 1999,[18] Bergman and Fel showed that composite material structures can improve the power factor over the constituent components. In these classical models, the nanoscale effects were not taken into account. Mingo *et al.*[1] performed semiclassical electron and phonon transport calculations on nanocomposite alloys of silicide nanoparticles embedded in SiGe. They considered the wavelength

[a]Author to whom correspondence should be addressed. Electronic mail: dvashae@ncsu.edu. Tel.: (919) 515-9599.

TABLE I. Stoichiometry of the powders and preparation parameters.

Name	Dopant, at. %	Composition	Milling time (h)
$FeSi_2$	Cu, 1%	$Fe_{0.34}Si_{0.66}$	50
Mg_2Si	Bi, 2%	$Mg_{0.67}Si_{0.33}$	23
SiGe	P, 2%	$Si_{0.88}Ge_{0.12}$	65
SiGe–$FeSi_2$	P, 2%–Cu, 1%	$(Si_{0.88}Ge_{0.12})_{0.925}$–$(Fe_{0.34}Si_{0.66})_{0.05}$–$Ag_{0.025}$	50
SiGe–Mg_2Si	P, 2%–Bi, 5%	$(Si_{0.88}Ge_{0.12})_{0.95}$–$(Mg_{0.67}Si_{0.33})_{0.05}$	20

dependent relaxation times and showed that significant ZT enhancement is possible mainly due to the reduction of the lattice thermal conductivity. They investigated both semiconductor and metallic nanoparticles embedded in SiGe host alloy and showed that the thermal conductivity has a minimum with respect to the nanoparticle size, although the minimum is very wide and the thermal conductivity remains small for a wide range of nanoparticle sizes. Both types of nanoparticles in the range of approximately 3-30 nm reduce the thermal conductivity considerably.

In this paper, the experimental data from bulk nanostructured SiGe, $FeSi_2$, and Mg_2Si along with nanocomposites of SiGe with embedded Mg_2Si and $FeSi_2$ nanoinclusions are presented and compared with each other. Mg_2Si and SiGe–$FeSi_2$ data are reported from previous studies Refs. 19 and 20, respectively, to compare with the single phase $FeSi_2$ and nanocomposite SiGe–Mg_2Si thermoelectric properties. All materials were synthesized via similar powder metallurgy/sintering process and their properties were measured using similar instruments, which assured a fair comparison of the results. The results showed that a significant reduction of the thermal conductivity is possible in both nanostructured SiGe and silicide–SiGe nanocomposites compared to polycrystalline SiGe. Both semiconductor silicide (Mg_2Si–SiGe) and metal silicide ($FeSi_2$–SiGe) nanocomposites showed smaller thermal conductivity compared with nanostructured SiGe resulting in higher ZT.

All the materials were processed starting from elements including Si (99% purity), Ge (99% purity), P (99.9% purity), Mg (99.99% purity), Bi (99.9% purity), Fe (99.9% purity), Cu (99.9% purity), and Ag (99.9% purity). The silicide alloys of $Si_{0.88}Ge_{0.12}$, $FeSi_2$, and Mg_2Si were separately prepared in powder form using high energy ball milling according to the stoichiometric ratio listed in Table I. P, Cu, and Bi were used as n-type dopant in SiGe, $FeSi_2$, and Mg_2Si powders, respectively. The elements for each composition were weighted and loaded in a tungsten carbide bowl along with tungsten carbide balls. The bowl was sealed inside an argon filled glove box and the load was subsequently milled in a planetary ball mill (Fritsch-P7PL) at 1000 rpm. The milling time for each material is listed in Table I. Once the SiGe, Mg_2Si, and $FeSi_2$ alloys were ready, their powders were weighted according to the formula listed in Table I and milled to prepare the SiGe–$FeSi_2$ and SiGe–Mg_2Si nanocomposites.

The powders were compacted and sintered in a graphite die with an internal diameter of 12.7 mm. The sintering was performed using a customized hot press system that heated the sample by sending a large direct current (500 A-1000 A) into the die, which resulted in rapid consolidation of the power. The hot press temperature was precisely monitored using a k-type thermocouple placed in the graphite die close to the middle of the sample. Numerous samples were synthesized and characterized in order to optimize the sintering conditions and attain the highest possible ZT. The main sintering parameters include the sintering temperature, soaking time, and the pressure. Table II shows the optimized sintering parameters along with mass density, thermal conductivity (at maximum ZT), and maximum ZT of SiGe, $FeSi_2$, Mg_2Si, SiGe–$FeSi_2$, and SiGe–Mg_2Si samples. The data related to the thermal conductivity and ZT will be discussed in detail later.

The microstructure and distribution of the elements in the samples were characterized by a Hitachi S-400 scanning electron microscope (SEM), equipped with an Oxford Instruments energy dispersive spectrometer (EDS), and transmission electron microscope (TEM, JEOL-JEM-2100). For atomic resolution and phase/element identification, bulk samples were mechanically polished using an Allied Multiprep polishing system and then ion milled using a Fischione Model 1050 Ion Mill. A probe-corrected FEI Titan G2 60-300 kV scanning transmission electron microscope (STEM) equipped with an X-FEG source and Super-X™ EDS detector was operated at 200 kV

TABLE II. Sintering parameters, density, thermal conductivity, and maximum ZT of the synthesized materials.

Name	Sintering Temp. (°C)	Soak time (min)	Density (g/cm^3)	Density (% of full density)	Temperature at max ZT (°C)	Thermal conductivity at max ZT (W/mK)	Max ZT	Ref.
$FeSi_2$	1100	6	4.43	93	665	3.7	0.2	This work
Mg_2Si	800	10	2.00	100	655	3.1	0.6	19
SiGe	1100	6	2.59	95	860	3.1	0.9	This work
SiGe–$FeSi_2$	1000	15	2.62	87	800	2.8	1.2	20
SiGe–Mg_2Si	1250	15	2.55	95	950	2.7	1.3	This work

for both imaging and EDS mapping. Other operating conditions included a 20 mrad probe forming convergence angle with 50 pA and 150 pA probe currents for imaging and EDS mapping, respectively. EDS maps were acquired and processed using the Bruker Espirit software.

The electrical resistivity and Seebeck coefficient of the samples were simultaneously measured using the commercially available Ulvac instrument, ZEM-3, from room temperature to 950 °C. The thermal diffusivities (α) were measured by laser flash, Netzsch's LFA 457 MicroFlash, in the range of 25-950 °C. The thermal conductivity (κ) was subsequently calculated according to $\kappa = \alpha\rho C_p$, where ρ is the mass density, measured by Archimedes method, and C_p is the specific heat, determined through a comparative method with Pyroceram reference sample in the laser flash apparatus.

Figure 1(a) shows the SEM image and the EDS map of an unpolished cleaved surface of SiGe–$FeSi_2$ sample. Small bright particles can be seen uniformly dispersed in the SiGe matrix. The EDS maps of the elements show a distribution of large Fe-rich particles (the bright particles in the SEM image) indicating the dispersion of $FeSi_2$ nanoinclusions in the matrix. The sintering temperature (1000 °C) of SiGe–$FeSi_2$ was higher than the melting point of silver (~960 °C) and below the melting point of $FeSi_2$ (~1220 °C); therefore, silver melts during the sintering, but $FeSi_2$ remains in a particulate form. The dark spots in EDS map images are due to the surface roughness of the samples. Figure 1(b) shows the bright field TEM image of SiGe–$FeSi_2$ sample. One can see a number of dispersed $FeSi_2$ nanoinclusions (~10 nm in size) in the matrix indicating the nanocomposite structure of SiGe matrix with embedded $FeSi_2$. As discussed, according to Ref. 20, nanoparticles in the range of 3-30 nm can efficiently scatter phonons and reduce the thermal conductivity of the sample.

The SiGe–Mg_2Si microstructure was imaged using high angular annular dark-field (HAADF) STEM, Figure 2(a). The corresponding EDS maps reveal the chemical distribution throughout the microstructure. SiGe–Mg_2Si sample demonstrated a granular structure of SiGe with Mg_2Si nanoinclusions. The Mg_2Si crystallites have sizes mostly from ~100 nm to ~400 nm. SiGe grain size has a random distribution mostly from ~150 nm to ~500 nm. However, TEM image (Figure 2(c)) shows additional high angle grain boundaries, which are known as internal grain boundary or twin boundary interfaces, caused by crystal defects. The presence of both grain boundaries and crystal defects serves to increase the number of phonon scattering centers and reduces the thermal conductivity. The larger size of the SiGe grains, compared to previously reported grain sizes in nanostructured SiGe,[21] is associated with the high sintering temperature, i.e., 1250 °C.

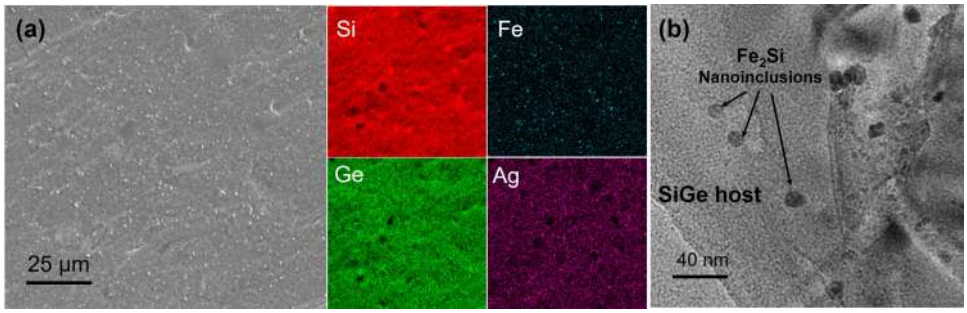

FIG. 1. (a) SEM image and EDS map of SiGe–$FeSi_2$ sample. The uniform dispersion of Fe indicates the presence of $FeSi_2$ nanoinclusions in the matrix. (b) TEM image of a similar sample showing nanoparticles of approximately 10 nm.

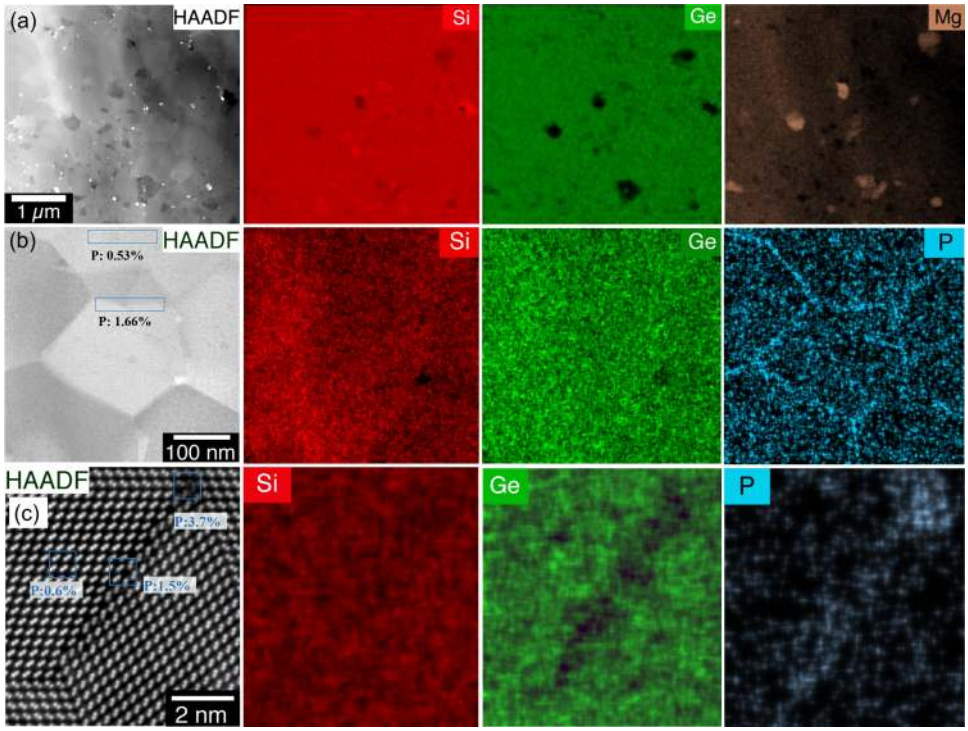

FIG. 2. (a) HAADF STEM and EDS maps corresponding to the elements identified in the SiGe–Mg_2Si sample, (b) higher concentration of P is shown at the grain boundaries, and (c) atomic resolution of an internal grain boundary showing phosphorous clustering near the interface.

Figure 2(b) shows a higher magnification image of SiGe–Mg_2Si sample. One can see several SiGe grains with an average atomic percent of 88.22 ± 1.81 Si and 11.79 ± 2.77 Ge. More importantly, the EDS map shows that phosphorous atoms have higher concentration at SiGe grain boundaries. While the P concentration inside the grain is approximately 0.5%, it has increased to ~1.7% near the grain boundary region. The larger concentration of P atoms near grain boundary could be both constructive and destructive in terms of thermoelectric properties. If the P atoms are solved in the lattice and are activated, the carrier concentration, and hence the Fermi energy, will increase near the grain boundary region. Therefore, the electrons will have higher energy and experience smaller scattering from the grain boundary potential. However, if P concentration is more than its solubility limit in the lattice, the atoms will precipitate and introduce additional grain boundary coulomb potential which can scatter charge carriers. Hence, a reduction of the charge carrier mobility occurs.[22] Therefore, there is an optimum P concentration that can improve the grain boundary transport characteristics. Since the solubility of P in Si is approximately 1.6% at 1000 °C,[23] it is expected that most of the P atoms at the grain boundary region are solved and activated. Therefore, the high concentration of P atoms, i.e., ~1.7%, is close to the optimum concentration and should minimize the grain boundary scattering.

A similar trend was observed for the internal grain boundaries as shown in the high magnification STEM EDS mapping of the internal grains in Figure 2(c). In order to obtain this image, the sample drift distortion was corrected using revolving STEM technique[24] to clearly resolve the structure of the grain boundary interface. These grains are formed inside the larger grains which are shown in Figure 2(b). They are resulted from a network of SiGe ⟨110⟩ twins. Although electron channeling may affect quantitative analysis,[25] a similar trend is observed that P content increases at regions with a higher structural disorder. The Si and Ge signals decreased at the interface, but P signal increased indicating a higher concentration of P at the interface. The measured P content is 0.6 at. %, 1.5 at. % ,and 3.7 at. % within the grain, at the internal grain boundary, and at the triple grain boundary point, respectively. Due to the observed high degree of lattice order near this

interface, P atoms are substitutionally located in the lattice at this specific grain interface, which indicates that they are likely activated and contribute to the carrier concentration.

Figure 3 compares the electrical conductivity, Seebeck coefficient, power factor times temperature (PFT), thermal conductivity, and dimensionless thermoelectric figure-of-merit (ZT) of β-$FeSi_2$, Mg_2Si, SiGe, SiGe–$FeSi_2$, SiGe–Mg_2Si, and crystalline n-type $Si_{0.80}Ge_{0.20}$ used in radioisotope thermoelectric generators (RTGs)[26] as functions of temperature. The representative sample from each material composition was selected from a large number of synthesized samples. These samples are divided into three groups; group 1: $FeSi_2$ and Mg_2Si, group 2: nanostructured SiGe and RTG SiGe, and group 3: nanocomposites of SiGe–$FeSi_2$ and SiGe–Mg_2Si. The thermoelectric properties of each group will be discussed separately as following:

Group 1. The electrical conductivity of β-$FeSi_2$ increased with temperature indicating the semiconductor β phase and non-degenerate (low) carrier concentration of the sample. Cu is the n-type dopant for $FeSi_2$ and results in a negative Seebeck coefficient. The absolute value of the Seebeck coefficient increased up to 600 °C, then, it reduced at higher temperatures. The PFT of β-$FeSi_2$

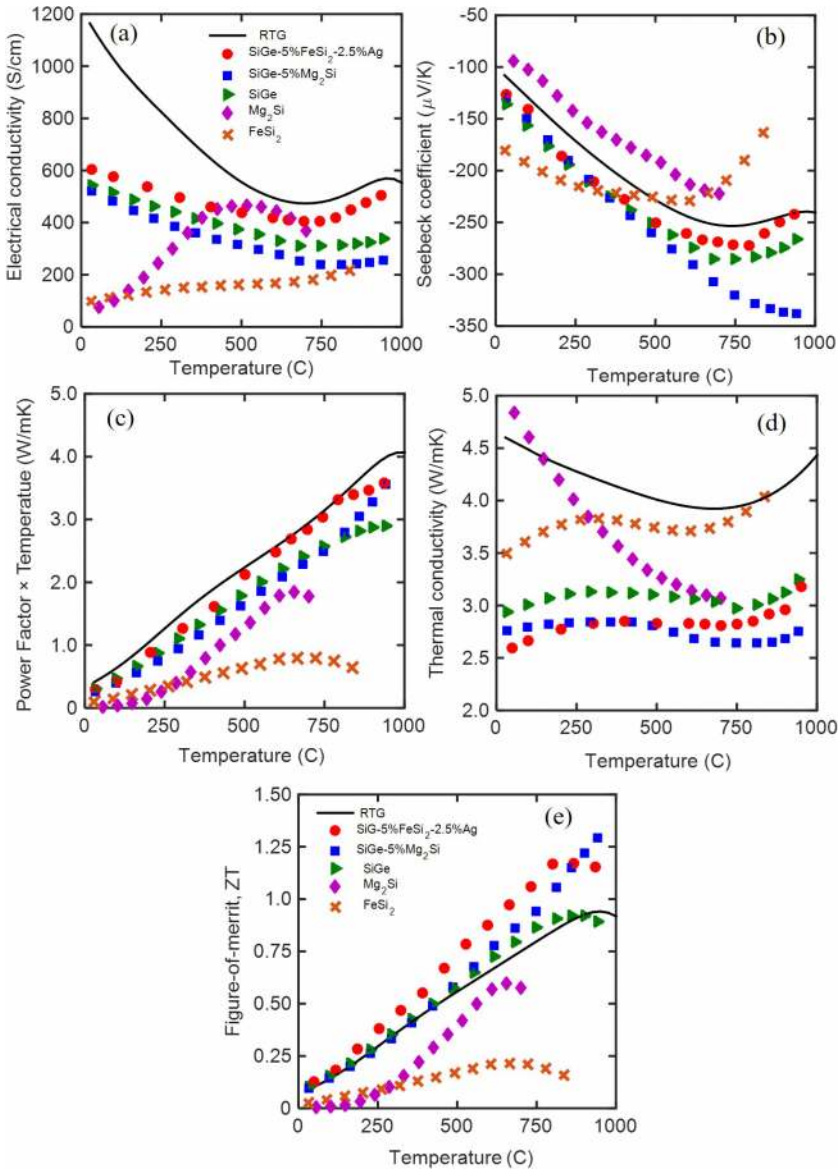

FIG. 3. (a) Electrical conductivity, (b) Seebeck coefficient, (c) PFT, (d) Thermal conductivity and (e) ZT of $FeSi_2$, Mg_2Si, SiGe, and nanocomposites of SiGe–$FeSi_2$ and SiGe–Mg_2Si all in symbols. The solid line shows the data of the RTG sample.

increased with temperature and reached a maximum at ~700 °C above which the PFT reduced due to the bipolar contribution from the thermal carriers. The contribution of the thermal carriers is confirmed by the faster increase of the electrical conductivity, the reduction of the Seebeck coefficient and the increase of the thermal conductivity near 600-700 °C. The positive slope of the thermal conductivity vs temperature below ~300 °C is due to the phonon grain boundary scattering and phonon-electron scattering. As the temperature increases above 300 °C, the 3-phonon scattering dominates and the thermal conductivity starts to decrease with temperature. The thermal conductivity increases again above 600 °C, which is due to the bipolar thermal diffusion as mentioned before. The peak ZT of $FeSi_2$ is ~0.2 at 700 °C which is the lowest ZT in comparison to the other samples.

The electrical conductivity of Mg_2Si increases with temperature up to ~550 °C, then decreases with further temperature increase (Figure 3(a)). The low temperature characteristic of Mg_2Si is compatible with very low doped Mg_2Si while the high temperature behavior is matched with highly doped one. The negative sign of the Seebeck coefficient of Mg_2Si (Figure 3(b)) confirms the n-type behavior of Bi dopant and illustrates the normal behavior of highly doped Mg_2Si due to the small absolute value of Seebeck coefficient at room temperature, similar to the reported results by You and Kim.[27] The low temperature behavior of electrical conductivity might be due to the lower amount of activated dopant in Mg_2Si. The PFT of Mg_2Si increases with temperature up to 650 °C due to the increase in both electrical conductivity and absolute Seebeck coefficient. Further increase in temperature reduces the PFT due to strong reduction of the electrical conductivity. The thermal conductivity of Mg_2Si decreases from 4.8 W/mK at room temperature to 3 W/mK at 700 °C due to the 3-phonon scattering. Mg_2Si has a very small value of ZT at room temperature which increases with temperature and reaches a maximum of 0.6 at 650 °C.

Group 2. The electrical conductivity of SiGe decreased with temperature due to the reduction of carrier mobility caused by the electron-phonon scattering at higher temperatures up to 750 °C.[9] Above 750 °C, intrinsic conduction slightly increased the electrical conductivity. The electrical conductivity of SiGe is smaller than RTG SiGe in all temperature ranges; however, the difference reduces at temperatures above 450 °C. This can be associated with the grain boundary scattering of the charge carriers in the nanostructured SiGe sample. In RTG SiGe, ionized impurities control the electron mobility at room temperature, while in nanostructured SiGe grain boundary scattering is dominant at room temperature.[9] At high temperatures, electron-phonon scattering mechanism predominates in both RTG SiGe and nanostructured SiGe; consequently, the charge carrier mobility is affected significantly by acoustic phonon scattering in both samples, which explains their smaller difference at high temperatures.

In comparison to RTG SiGe, the absolute Seebeck coefficient of nanostructured SiGe is higher at all temperatures and the difference is approximately uniform. This is due to the smaller carrier concentration in nanostructured SiGe which also explains its lower electrical conductivity. The PFT of nanostructured SiGe is smaller than RTG SiGe sample at all temperatures which is due to its significantly smaller electrical conductivity. This difference increases with temperature resulting in ~25% smaller PFT at 950 °C in the nanostructured SiGe sample compared to the RTG SiGe.

The thermal conductivity of SiGe follows the same trend as that of $FeSi_2$. The justification is also the same which is the overall reduction of thermal conductivity due to 3-phonon scattering and increase at above 750 °C due to the ambipolar thermal conduction.[28] The remarkable drop in the thermal conductivity of nanostructured SiGe in comparison to the RTG SiGe over the entire temperature range is due to the grain boundary scattering. It should be considered that due to the higher amount of Ge in the RTG alloy, i.e., $Si_{0.80}Ge_{0.20}$, the thermal conductivity should be theoretically smaller than that of crystalline $Si_{0.88}Ge_{0.12}$.[29] Nevertheless, the grain boundary scattering has compensated the increase due to the smaller content of Ge and has further reduced the thermal conductivity. The drop of the thermal conductivity is ~36% at room temperature and 24% at 950 °C.

The ZT of nanostructured n-type SiGe follows a similar trend as that of RTG SiGe. Although the thermal conductivity of the nanostructured SiGe sample dramatically decreased, ZT remains almost equal due to simultaneous reduction of the PFT. Therefore, in order to enhance the ZT of n-type SiGe, other methods that can reduce the thermal conductivity more than the power factor are required.

Nanoparticles can reduce the thermal conductivity below the alloy limit by enhancing the scattering centers.[30] In brief, the cluster of N atoms of a second phase embedded in a matrix

can scatter low frequency and high frequency phonons by factors of N^2 and $N^{2/3}$, respectively.[11] Accordingly, low frequency phonons are more affected by clustering than high frequency phonons. In an alloy, the high frequency phonons are already scattered strongly by point defects;[30] therefore, the cluster of N atoms can further reduce the thermal conductivity by simultaneous scattering of the low frequency phonons in the lattice. Such a cluster of the atoms, i.e., nanoparticles, can also scatter the electrons; however, it is often smaller than the sum of other scatterings in highly doped thermoelectric materials.[9] As a result, the reduction of the electrical conductivity can be less than the reduction of the thermal conductivity. Based on similar arguments, it was suggested by Mingo *et al.*[1] that nanoinclusions in SiGe alloy can maintain the PFT while reducing the thermal conductivity resulting in ZT improvement.

Group 3. Figure 3 shows that the electrical conductivity of SiGe, SiGe–$FeSi_2$, and SiGe–Mg_2Si samples follows the general behavior that was discussed for SiGe. Compared to RTG SiGe, the electrical conductivity is smaller due to the electron scattering by the grain boundaries.

SiGe–$FeSi_2$ with 2.5% silver has the highest electrical conductivity, which can be associated with its higher carrier concentration and/or carrier mobility. The 2.5% silver acted as sintering aid and allowed improving the bonding of the grains while maintaining a low sintering temperature. During the hot pressing, silver melts at ~960 °C and fills the pores among the grains, which can improve the electrical contact at the grain boundaries; hence, it improved the overall carrier mobility. The common trend of the electrical conductivity reduction with temperature for all the samples is associated with the reduction of the carrier mobility due to the elevation of the acoustic phonon scattering.

The absolute values of the Seebeck coefficients for the nanocomposite samples are larger than that of the RTG SiGe sample, which indicates their lower carrier concentration. The EDS map of SiGe–$Mg_{20}Si$ sample (Figure 2) shows strong precipitation of phosphorous at grain boundary regions. Therefore, it is expected that the sample should have a lower concentration of active dopants, which can explain its higher absolute Seebeck coefficient and lower electrical conductivity compared to the RTG SiGe sample.

The Seebeck coefficient of the three SiGe, SiGe–$FeSi_2$, and SiGe–Mg_2Si samples are almost similar up to ~500 °C, which indicates their similar carrier concentrations. At above ~500 °C, the absolute Seebeck coefficients of the nanostructured SiGe and SiGe–$FeSi_2$ saturated and then decreased with temperature. This can be associated with the onset of the bipolar transport due to the elevated thermal excitations at high temperatures.[21] However, the absolute Seebeck coefficient of SiGe–Mg_2Si sample continued increasing with temperature up to ~1000 °C. Since the samples have similar carrier concentration and band gap energy, the lack of or smaller bipolar effect in SiGe–Mg_2Si sample indicates that the holes (minority carriers) have smaller mobility in this sample. This can be associated with the preferentially higher scattering of the minority carriers by the Mg_2Si nanoinclusions or the grain boundaries in this sample.[31]

Moreover, dopant activation in SiGe samples often increases the carrier concentration at high temperatures, which depends on the concentration of the precipitated dopants in the sample.[9,32] This is usually observed through the increase of the electrical conductivity and decrease of the absolute Seebeck coefficient. However, it does not strongly affect the thermal conductivity because the electronic thermal conductivity reduces with temperature and becomes negligible at high temperatures. Therefore, the thermal conductivity increase in SiGe and SiGe–$FeSi_2$ sample at above ~750 °C must be more due to the bipolar transport than the dopant activation.

It should be noted that for RTG SiGe sample these trends start at slightly lower temperatures (~700 °C) which is due to the smaller bandgap of $Si_{0.80}Ge_{0.20}$ used in RTG sample than $Si_{0.88}Ge_{0.12}$ used in this study.

The PFTs of the nanostructured SiGe and the nanocomposite samples are smaller than that of the RTG SiGe. From room temperature to ~400 °C, PFT of the SiGe and the nanocomposite samples are similar. The PFTs of SiGe and SiGe–Mg_2Si are similar up to 800 °C and start to deviate at higher temperatures. The PFT of the SiGe–$FeSi_2$ is the highest among the samples over the wide temperature range (~500-950 °C) due to its higher electrical conductivity.

The thermal conductivities of the nanocomposites SiGe–$FeSi_2$ and SiGe–Mg_2Si are lower than those of nanostructured SiGe and RTG SiGe. At room temperature, the thermal conductivity of

the nanocomposite samples are similar to that of amorphous silicon,[33] which, as discussed, can be associated with the scattering of the acoustic phonons at interfaces of the silicide nanoinclusions. According to Mingo *et al.*,[1] both metal and semiconductor nanoinclusions in $Si_{0.5}Ge_{0.5}$ alloy matrix were predicted to have a minimum lattice thermal conductivity of approximately 1.5 W/mK at room temperature. According to our measurements, the lattice thermal conductivities of Mg_2Si–$Si_{0.88}Ge_{0.12}$ and $FeSi_2$–$Si_{0.88}Ge_{0.12}$ nanocomposites at room temperature are approximately 2.3 W/mK and 2.0 W/mK, respectively (using Wiedemann–Franz law to separate the electronic part of the thermal conductivity). The small difference between the theoretical predictions and our data can be partly associated with the smaller thermal conductivity of $Si_{0.5}Ge_{0.5}$ (~7 W/mK) compared to $Si_{0.88}Ge_{0.12}$ (~10 W/mK).[29] It should be also noted that $Si_{0.80}Ge_{0.20}$ has a smaller lattice thermal conductivity than $Si_{0.88}Ge_{0.12}$ (8.5 W/mK compared to 7 W/mK, respectively[29]). However, the $Si_{0.88}Ge_{0.12}$–Mg_2Si and $Si_{0.88}Ge_{0.12}$–$FeSi_2$ nanocomposites showed a smaller thermal conductivity than RTG $Si_{0.80}Ge_{0.20}$ alloy indicating that nanostructuring can compensate for the effect of the smaller amount of Ge in the alloy. The thermal conductivity reduced with temperature up to ~750 °C due to the enhancement of the 3-phonon scattering. Above 750 °C, the polar thermal diffusion increases the thermal conductivity. The smaller thermal conductivity at higher temperatures for SiGe–Mg_2Si, confirms that Mg_2Si nanoinclusions are more effective than $FeSi_2$ in scattering of the minority carrier. It should be also noted that, since silver was added to SiGe–$FeSi_2$, there may be additional scattering at silver interfaces contributing in reducing the thermal conductivity.

Figure 3(e) shows the comparison of the ZT values versus temperature for the samples. ZT of SiGe–$FeSi_2$ is higher than RTG sample in most of the temperature range reaching ZT ~ 1.2 over the temperature range of 800-950 °C. SiGe–Mg_2Si has the highest ZT ~ 1.3 at 950 °C which is 45% higher than RTG sample. The ZT seems to be increasing with temperature above 950 °C, which was not measured due to the limitations of the measuring instruments. The comparisons of Figures 3(c)–3(e) indicates that the ZT enhancement in SiGe–$FeSi_2$ is associated with the reduction of the thermal conductivity while maintaining almost similar PFT as that of the RTG SiGe. SiGe–Mg_2Si sample showed the smallest thermal conductivity at high temperatures which resulted in the highest ZT at above 870 °C although its PFT was smaller than that of SiGe–$FeSi_2$. Both nanocomposite samples, compared with nanostructured SiGe, showed higher ZT mainly due to their smaller thermal conductivity while maintaining a similar or higher thermoelectric power factor.

Nanostructured silicides of $FeSi_2$, Mg_2Si, and $Si_{0.88}Ge_{0.12}$, along with their nanocomposites of $Si_{0.88}Ge_{0.12}$–$FeSi_2$ and $Si_{0.88}Ge_{0.12}$–Mg_2Si were developed by rapid hot pressing and their nanostructural, electrical, and thermal properties were compared. A large number of samples were synthesized, measured, and analyzed for each material structure in order to optimize the sintering parameters and the thermoelectric properties. The thermoelectric properties of the samples were compared with those of the n-type SiGe used in a radioisotope thermoelectric generator (RTG). The addition of silicide nanoinclusions to SiGe alloy maintained or increased the power factor compared with that of the nanostructured SiGe while reducing the thermal conductivity. These results confirm the concept of silicide nanoparticle in SiGe alloy proposed earlier by Mingo *et al.*[1] suggesting a new approach for making efficient thermoelectric materials. Compared to RTG SiGe, the thermal conductivity of the nanocomposite samples reduced by nearly 45%. The ZT of both nanocomposite samples was higher than those of RTG SiGe and nanostructured SiGe in a wide temperature range. In $Si_{0.88}Ge_{0.12}$–Mg_2Si nanocomposite ZT ~ 1.3 was achieved. $Si_{0.88}Ge_{0.12}$–$FeSi_2$ showed ZT enhancement over the largest range of temperature reaching ZT > 1 at above 670 °C and ZT ~ 1.2 over 800-950 °C. All the nanocomposite samples utilized a smaller amount of germanium compared to RTG SiGe which reduced the material cost.

This study is partially based upon work supported by Air Force Office of Scientific Research (AFOSR) under Contract No. FA9550-12-1-0225 and the National Science Foundation (NSF) under Grant Nos. EEC-1160483, ECCS-1351533 and CMMI-1363485. J.S.K. acknowledges the funding support from Oklahoma Center for the Advancement of Science & Technology (OCAST) Oklahoma Applied Research Support (OARS) program under Contract No. AR14-052.

This work was performed in part at the Analytical Instrumentation Facility (AIF) at North Carolina State University, which is supported by the State of North Carolina and the National Science

Foundation (award number ECCS-1542015). The AIF is a member of the North Carolina Research Triangle Nanotechnology Network (RTNN), a site in the National Nanotechnology Coordinated Infrastructure (NNCI).

[1] N. Mingo, D. Hauser, N. P. Kobayashi, M. Plissonnier, and A. Shakouri, ""Nanoparticle-in-alloy" approach to efficient thermoelectrics," Nano Lett. **9**(2), 711–715 (2009).
[2] L. D. Hicks and M. S. Dresselhaus, "Effect of quantum-well structures on the thermoelectric figure of merit," Phys. Rev. B **47**, 12727 (1993).
[3] D. M. Rowe, *Thermoelectrics Handbook: Macro to Nano* (CRC Press, 2005).
[4] C. B. Vining, *Handbook of Thermoelectrics* (CRC, New York, 1995).
[5] F. Xiao, C. Hangarter, B. Yoo, Y. Rheem, K. H. Lee, and N. V. Myung, "Recent progress in electrodeposition of thermoelectric thin films and nanostructures," Electrochim. Acta **53**, 8103–8117 (2008).
[6] N. Satyala, P. Norouzzadeh, and D. Vashaee, "Nano bulk thermoelectrics: Concepts, techniques, and modeling," in *Nanoscale Thermoelectrics* (Springer International Publishing, 2014), pp. 141–183.
[7] B. Poudel, Q. Hao, Y. Ma, Y. Lan, A. Minnich, B. Yu, X. Yan, D. Wang, A. Muto, D. Vashaee, X. Chen, J. Liu, M. S. Dresselhaus, G. Chen, and Z. Ren, "High-Thermoelectric Performance of Nanostructured Bismuth Antimony Telluride Bulk Alloys," Science **320**, 634 (2008).
[8] S. K. Bux, R. G. Blair, P. K. Gogna, H. Lee, G. Chen, M. S. Dresselhaus, R. B. Kaner, and J. P. Fleurial, "Nanostructured bulk silicon as an effective thermoelectric material," Adv. Funct. Mater. **19**, 2445–2452 (2009).
[9] A. J. Minnich, H. Lee, X. W. Wang, G. Joshi, M. S. Dresselhaus, Z. F. Ren, G. Chen, and D. Vashaee, "Modeling study of thermoelectric SiGe nanocomposites," Phys. Rev. B **80**(15), 155327 (2009).
[10] K. Biswas, J. He, I. D. Blum, C. Wu, T. P. Hogan, D. N. Seidman, V. P. Dravid, and M. G. Kanatzidis, "High-performance bulk thermoelectrics with all-scale hierarchical architectures," Nature **489**(7416), 414–418 (2012).
[11] N. Satyala and D. Vashaee, "The effect of crystallite size on thermoelectric properties of bulk nanostructured magnesium silicide (Mg_2Si) compounds," Appl. Phys. Lett. **100**, 073107 (2012).
[12] N. Satyala and D. Vashaee, "Detrimental influence of nanostructuring on the thermoelectric properties of magnesium silicide," J. Appl. Phys. **112**(9), 093716 (2012).
[13] M. Mohebali, Y. Liu, L. Tayebi, J. S. Krasinski, and D. Vashaee, "Thermoelectric figure of merit of bulk $FeSi_2$−$Si_{0.8}Ge_{0.2}$ nanocomposite and a comparison with β-$FeSi_2$," Renewable Energy **74**, 940–947 (2015).
[14] P. Norouzzadeh, Z. Zamanipour, J. S. Krasinski, and D. Vashaee, "The effect of nanostructuring on thermoelectric transport properties of p-type higher manganese silicide $MnSi_{1.73}$," J. Appl. Phys. **112**(12), 124308-1–124308-7 (2012).
[15] Z. Zamanipour, X. Shi, M. Mozafari, J. S. Krasinski, L. Tayebi, and D. Vashaee, "Synthesis, characterization, and thermoelectric properties of nanostructured bulk p-type $MnSi_{1.73}$, $MnSi_{1.75}$, and $MnSi_{1.77}$," Ceram. Interfaces **39**(3), 2353–2358 (2013).
[16] J. P. Straley, "Thermoelectric properties of inhomogeneous materials," J. Phys. D: Appl. Phys. **14**, 2101 (1981).
[17] D. J. Bergman and O. Levy, "Thermoelectric properties of a composite medium," J. Appl. Phys. **70**, 6821 (1991).
[18] D. J. Bergman and L. J. Fel, "Enhancement of thermoelectric power factor in composite thermoelectrics," J. Appl. Phys. **85**, 8205 (1999).
[19] N. Satyala, J. S. Krasinski, and D. Vashaee, "Simultaneous enhancement of mechanical and thermoelectric properties of polycrystalline magnesium silicide with conductive glass inclusion," Acta Mater. **74**, 141–150 (2014).
[20] A. Nozariasbmarz, Z. Zamanipour, P. Norouzzadeh, J. S. Krasinski, and D. Vashaee, "Enhanced thermoelectric performance in metal/semiconductor nanocomposite of iron silicide/silicon germanium," RSC Adv. **6**, 49643 (2016).
[21] Z. Zamanipour, X. Shi, A. M. Dehkordi, J. S. Krasinski, and D. Vashaee, "The effect of synthesis parameters on transport properties of nanostructured bulk thermoelectric p-type silicon germanium alloy," Phys. Status Solidi A **209**(10), 2049–2058 (2012).
[22] C. H. Seager and T. G. Castner, "Zero-bias resistance of grain boundaries in neutron-transmutation-doped polycrystalline silicon," J. Appl. Phys. **49**, 3879 (1978).
[23] F. A. Trumbore, "Solid solubilities of impurity elements in germanium and silicon," Bell Syst. Tech. J. **39**, 205 (1960).
[24] X. Sang and J. M. LeBeau, "Revolving scanning transmission electron microscopy: Correcting sample drift distortion without prior knowledge," Ultramicroscopy **138**, 28–35 (2014).
[25] Z. Yu, D. A. Muller, and J. Silcox, "Effects of specimen tilt in ADF-STEM imaging of a-Si/c-Si interfaces," Ultramicroscopy **108**, 494–501 (2008).
[26] G. Joshi, H. Lee, Y. Lan, X. Wang, G. Zhu, D. Wang, R. W. Gould, D. C. Cuff, M. Y. Tang, M. S. Dresselhaus, G. Chen, and Z. Ren, "Enhanced Thermoelectric Figure-of-Merit in Nanostructured p-type Silicon Germanium Bulk Alloys," Nano Lett. **8**(12), 4670–4674 (2008).
[27] S. W. You and I. H. Kim, "Solid-state synthesis and thermoelectric properties of Bi-doped Mg_2Si compounds," Curr. Appl. Phys. **11**, S392–S395 (2011).
[28] D. P. White and P. G. Klemens, "Thermal conductivity of thermoelectric $Si_{0.8}$-$Ge_{0.2}$ alloys," J. Appl. Phys. **71**(9), 4258 (1992).
[29] J. Garg, N. Bonini, B. Kozinsky, and N. Marzari, "Role of disorder and anharmonicity in the thermal conductivity of silicon-germanium alloys: A first-principles study," Phys. Rev. Lett. **106**, 045901 (2011).
[30] J. M. Ziman, *Electrons and Phonons* (Oxford University Press, New York, 2001).
[31] J.-H. Bahk and A. Shakouri, "Enhancing the thermoelectric figure of merit through the reduction of bipolar thermal conductivity with heterostructure barriers," Appl. Phys. Lett. **105**, 052106 (2014).
[32] Z. Zamanipour, J. S. Krasinski, and D. Vashaee, "Comparison of boron precipitation in p-type bulk nanostructured and polycrystalline silicon germanium alloy," J. Appl. Phys. **113**(14), 143715 (2013).
[33] P. Norouzzadeh, A. Nozariasbmarz, J. S. Krasinski, and D. Vashaee, J. Appl. Phys. **117**, 214303 (2015).